
Advanced Composite Materials
Publication details, including instructions for authors and subscription information:
http://www.tandfonline.com/loi/tacm20

# Numerical simulation of microscopic damage and strength of fiber-reinforced plastic composites

T. Okabe [a], T. Motani, M. Nishikawa [b] & M. Hashimoto [c]

[a] Department of Aerospace Engineering, Tohoku University, 6-6-01 Aoba-yama, Aoba-ku, Sendai, 980-8579, Japan

[b] Department of Nanomechanics, Tohoku University, 6-6-01 Aoba-yama, Aoba-ku, Sendai, 980-8579, Japan

[c] Composite Materials Research Laboratories (CMRL), Toray Industries, Inc., 1515, Tsutsui, Masaki-cho, Iyogun, Ehime, 791-3193, Japan

Version of record first published: 29 Jun 2012.

To cite this article: T. Okabe, T. Motani, M. Nishikawa & M. Hashimoto (2012): Numerical simulation of microscopic damage and strength of fiber-reinforced plastic composites, Advanced Composite Materials, 21:2, 147-163

To link to this article: http://dx.doi.org/10.1080/09243046.2012.688495

*Advanced Composite Materials*
Vol. 21, No. 2, April 2012, 147–163



# Numerical simulation of microscopic damage and strength of fiber-reinforced plastic composites

T. Okabe[a]*, T. Motani, M. Nishikawa[b] and M. Hashimoto[c]

[a]*Department of Aerospace Engineering, Tohoku University, 6-6-01 Aoba-yama, Aoba-ku, Sendai 980-8579, Japan;* [b]*Department of Nanomechanics, Tohoku University, 6-6-01 Aoba-yama, Aoba-ku, Sendai 980-8579, Japan;* [c]*Composite Materials Research Laboratories (CMRL), Toray Industries, Inc., 1515, Tsutsui, Masaki-cho, Iyogun, Ehime 791-3193, Japan*

(*Received 28 February 2012; accepted 2 April 2012*)

Discontinuous fiber-reinforced composites have better productivity and formability than continuous fiber-reinforced composites. However, their strength is remarkably low. Thus, there is an urgent need to improve the strength of discontinuous fiber-reinforced plastic composites. In this study, we utilized a unit-cell model that considers microscopic damage including matrix cracking and fiber breaking, and incorporates constitutive laws of thermosetting resin or thermoplastic resin for the matrix. The tensile damage and strength of the composite were investigated for various fiber lengths and/or matrix properties. We compared the simulated strengths with experiments for carbon fiber-reinforced polypropylene. The effect of deformation rate on mechanical behavior was also investigated.

**Keywords:** fiber-reinforced composite material; microscopic damage; strength; discontinuous fiber; numerical analysis



## 1. Introduction

The production of fuel-efficient automobiles is of high interest because of unstable oil prices. Fuel-efficient automobiles can be manufactured in several ways, but reducing automobile weight is one of the most efficient ways to improve fuel efficiency. Two general approaches may be used to reduce this weight: effectively designing products to remove unnecessary components and using lightweight materials in the structural components. This latter approach is thought to be the best candidate because products are already being effectively designed. Currently, fiber-reinforced plastic composites show promise. For example, carbon fiber-reinforced plastic composites have been applied to new aircraft. In this aircraft application, continuous fiber-reinforced composites are used for the components of structures. However, discontinuous fiber-reinforced composites are widely applied in automobiles, since continuous fiber-reinforced composites have formability and cost performance problems. Because discontinuous fiber-reinforced composites are not as strong as continuous fiber-reinforced composites, discontinuous fiber-reinforced composites are applied to only components that do not carry much of a load. Thus, the strength of discontinuous fiber-reinforced composites must be improved.

For fiber-reinforced plastic composites, thermoplastic resin is applied to discontinuous fiber-reinforced composites and thermosetting resin is applied to continuous fiber-reinforced

*Corresponding author. Email: okabe@plum.mech.tohoku.ac.jp

ISSN 0924-3046 print/ISSN 1568-5519 online

http://dx.doi.org/10.1080/09243046.2012.688495
http://www.tandfonline.com

composites. These composites have been studied individually, but how the failure mode changes due to changes in matrix type and fiber length has not been determined.

Recently, we developed a new simulation scheme for a unit-cell model in order to analyze the microscopic damage and failure of fiber-reinforced composites [10–13]. In this study, we use this scheme to investigate changes in failure mode and tensile strength due to changes in matrix type and fiber length. We also compare our simulated results with those of experiments for discontinuous long carbon fiber-reinforced composites. Deformation rate dependence of composites is also investigated.

## 2. Computational modeling

### 2.1. Model

Tensile damage growth in fiber-reinforced composites is numerically simulated using a unit-cell model. Here, the concept and the structure of the unit-cell model are described briefly. Since it is very difficult to reproduce damage growth in composites using a whole composite model, a unit-cell model is widely used to analyze damage that is generated in composites. The periodic boundary condition is applied to the model in order to remove surficial effects. Figure 1 presents a schematic of the unit-cell model. This model, which includes fiber and matrix, is used to reproduce the damage growth in composites. In this analysis, the plane strain condition is assumed for this model. Here, the radius of fiber $\bar{r}_f$ is assigned to be half the real fiber radius in order to reproduce the stress recovery of a broken fiber. We have confirmed that the analyzed stress recovery for a broken fiber using this fiber radius agrees well with that of 3D analysis. Fiber and matrix are assumed to be an isotropic body. Here, nine-node isoparametric elements are used for the fiber and six-node triangular elements are

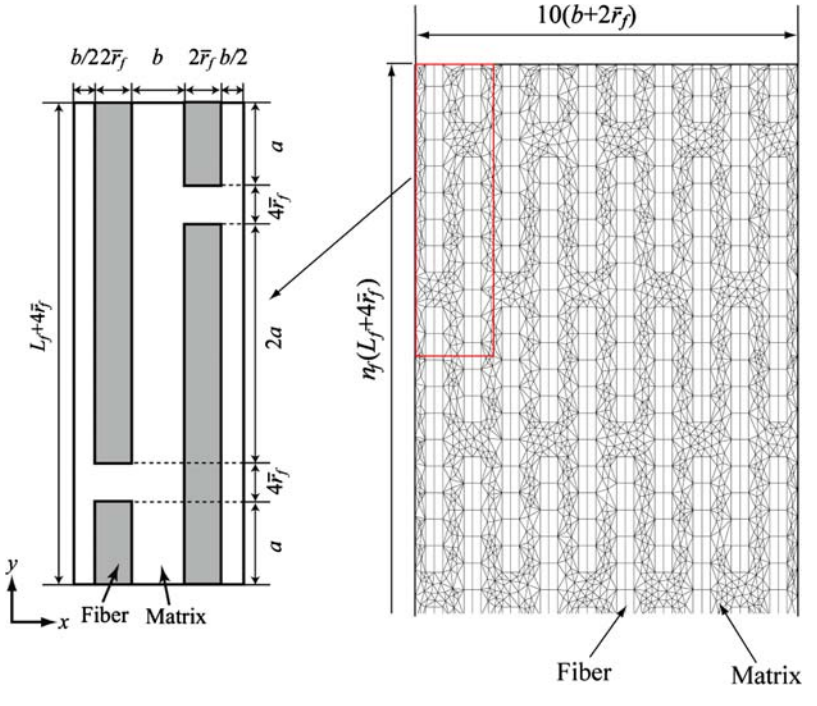


Figure 1. Unit-cell model for simulating the fracture of fiber-reinforced plastic.

used for the matrix. This model is based on the Huang-Talreja model [3], which analyzes the damage growth in a matrix using the Rice-Tracey model [17]. In this model, 10 fibers are aligned and the distance between them is calculated based on the fiber volume fraction. The distance between the up and down fibers is assumed to be $4\bar{r}_f$.

In unit-cell modeling, displacements and strain increments are divided into two parts, the global component and the local component:

$$\mathbf{u} = \mathbf{u}_G + \mathbf{u}_L, \tag{1}$$

$$\Delta\boldsymbol{\varepsilon} = \Delta\boldsymbol{\varepsilon}_G + \Delta\boldsymbol{\varepsilon}_L, \tag{2}$$

where the subscripts $G$ and $L$ denote the global and local components. The global strains are independent of the local coordinate in the unit cell, and they are assigned as constants. The volume average of strain $\boldsymbol{\varepsilon}$ for the unit cell should be equal to $\boldsymbol{\varepsilon}_G$. Thus, the volume average of strain $\boldsymbol{\varepsilon}_L$ in the unit cell must be zero.

### 2.2. Constitutive law for matrix

In this study, two types of matrix are addressed, thermosetting resin and thermoplastic resin. The constitutive law for thermosetting resin based on the continuum damage mechanics with damage parameter $D$ is given as follows [10]:

$$\Delta\boldsymbol{\sigma} = (1-D)\mathbf{C}^{ep} : \Delta\boldsymbol{\varepsilon} - \frac{\Delta D}{1-D}\boldsymbol{\sigma}, \tag{3}$$

$$\mathbf{C}^{ep} = \mathbf{C}^{e} - \frac{9\mu^2}{3\mu + H}\frac{1}{\bar{\sigma}^2}\boldsymbol{\sigma}' \otimes \boldsymbol{\sigma}', \tag{4}$$

where the elastic-plastic constitutive law based on the J2 flow is used. Here, $\boldsymbol{\sigma}$ is the stress tensor, $\mathbf{C}^e$ is the constitutive tensor, $\boldsymbol{\sigma}'$ is the deviatoric tensor, $\bar{\sigma}$ is the equivalent stress, $\mu$ represents the lame constants, and $H$ is the strain hardening parameter. In Equation (3), $D$ is the damage variable based on a strain-equivalent configuration, and it has a scalar quantity. This parameter enables us to account for matrix damage in the composites. We calculate the evolution of $D$ with the applied stress as

$$\Delta D = (1-D)C\left\langle \Delta\varepsilon_m^p \right\rangle + (B_0 + B_1 D)\Delta\bar{\varepsilon}^p, \tag{5}$$

$$C\left\langle \Delta\varepsilon_m^p \right\rangle = A\Delta\left[D\left(\frac{\langle\sigma_m\rangle}{\sigma_y}\right)^2\right]. \tag{6}$$

The first term represents the extension of existing voids or defects due to plastic volumetric expansion strain $\varepsilon_m^p$; and the second term represents damage extension due to shear failure. Here, $\sigma_m$ is the hydrostatic pressure. $A$ and $B$ denote dimensionless constants obtained by Nishikawa [10] and are listed in Table 1. The brackets $< >$ in Equation (5) are called as Macauley brackets. The meaning of the bracket $< >$ is $\langle X\rangle = X$ $(X \geq 0)$, 0 $(X<0)$.

Table 1. Material properties of epoxy matrix [13].

| | |
|---|---|
| Young's modulus $E_m$ | 3.4 GPa |
| Matrix Poisson's ratio $v_f$ | 0.31 |
| Yield stress $\sigma_y$ | 73 MPa |
| Hardening modulus $H$ | 76.7 MPa |
| Damage evolution law $A$ | 0.5 |
| $B_0$ | 0 |
| $B_1$ | 0.5 |
| $D_{\text{ini}}$ | 0.01 |

For the constitutive law of thermoplastic material, we utilized the constitutive model of a polypropylene (PP) matrix proposed by Kobayashi et al. [6]. They formulated a one-parameter damage mechanics model based on strain-equivalent configuration [8] to address the initiation and propagation of matrix cracks. We explain this constitutive model below. Within the framework of thermodynamics, the noncoaxial constitutive equation of a viscoplastic polymer with damage evolution is

$$\dot{\boldsymbol{\sigma}} = (1-D)\mathbf{C}_m^v : \dot{\boldsymbol{\varepsilon}} - (1-D)\frac{3\mu\dot{\bar{\varepsilon}}^p \cos\delta}{\bar{\sigma}}\boldsymbol{\sigma}' - \frac{\dot{D}}{1-D}\boldsymbol{\sigma}, \tag{7}$$

where

$$\mathbf{C}_m^v = \frac{H}{H+3\mu}\left[\mathbf{C}_m^e + \frac{3\mu}{H}\left\{\frac{3\lambda+2\mu}{3}\mathbf{I}\otimes\mathbf{I} + 3\mu\frac{\boldsymbol{\sigma}'\otimes\boldsymbol{\sigma}'}{\bar{\sigma}^2}\right\}\right],$$

$$H = \frac{1}{1-D}\frac{\dot{\bar{\sigma}}}{\dot{\bar{\varepsilon}}^p k}, \quad \bar{\sigma} = \sqrt{\frac{3}{2}\boldsymbol{\sigma}':\boldsymbol{\sigma}'}, \quad \dot{\bar{\sigma}} = \sqrt{\frac{3}{2}\dot{\boldsymbol{\sigma}}':\dot{\boldsymbol{\sigma}}'},$$

where $\boldsymbol{\sigma}$ is the stress tensor, $\boldsymbol{\varepsilon}$ is the strain tensor, $\boldsymbol{\sigma}'$ is the deviatoric stress, $\mathbf{C}_m^e$ is the fourth-order tensor of the elastic constitution law, $\lambda$ and μ denote Lamé constants, and $\dot{\bullet}$ denotes the time derivative. The equivalent strain rate $\dot{\bar{\varepsilon}}^p$ is defined by the following hardening rule for the PP matrix (Murakami et al. [9]):

$$\dot{\bar{\varepsilon}}^p = \dot{\varepsilon}_r\left(\frac{\bar{\sigma}}{g(\bar{\varepsilon}^p)}\right)^{\frac{1}{m}}, \tag{8}$$

where $g(\bar{\varepsilon}^p) = \sigma_r\{\tanh(k_1\bar{\varepsilon}^p) + k_2 + H_e(\bar{\varepsilon}^p - \varepsilon_r)k_3(\exp\bar{\varepsilon}^p - \exp\varepsilon_r)\}$, $m$ is the rate-sensitivity parameter, $\dot{\varepsilon}_r$ is the reference strain rate, $\varepsilon_r$ is the reference strain at rehardening, and $\sigma_r$ is the initial yield stress. In addition to these parameters, $k_1$, $k_2$, and $k_3$ are determined as material constants; and $H_e(\bullet)$ is the Heaviside step function. The noncoaxial angle $\delta$ in Equation (7) between deviatoric stress $\boldsymbol{\sigma}'$ and deviatoric plastic strain $\boldsymbol{\varepsilon}^{p\prime}$ changes with the varying direction of the rate $\dot{\boldsymbol{\sigma}}'$ of deviatoric stress, according to the following empirical relationship.

$$\sin\delta = k\sin\alpha, \tag{9}$$

$$k = \begin{cases} p_1\sin\left(\frac{\pi}{2}\frac{m}{p_2}\right) & (0 \le m \le p_2) \\ p_1\{\tanh[-p_3(m-p_2)]+1\} & (p_2 \le m) \end{cases}.$$

Here, $p_1$, $p_2$, and $p_3$ are material constants; $\alpha$ is the angle between deviatoric stress $\boldsymbol{\sigma}'$ and the rate $\dot{\boldsymbol{\sigma}}'$ of deviatoric stress and satisfies the following relationship.

$$\cos\alpha = \frac{\dot{\bar{\sigma}}}{\dot{\bar{\sigma}}}. \tag{10}$$

Finally, $D$ in Equation (7) denotes the damage variable causing stiffness degradation. Here, the damage variable is defined as a scalar quantity. Microscopic failure characteristics can be incorporated into the evolutionary equation of the damage variable. The following evolutionary equation of the damage variable is used to address crazing evolution and annihilation [6].

$$\dot{D} = A(1-D)\langle \dot{\varepsilon}_m^p \rangle + B\frac{\dot{\bar{\varepsilon}}^p}{\dot{\bar{\varepsilon}}^p}. \tag{11}$$

The first term represents craze growth due to plastic volumetric expansion strain $\varepsilon_m^p$ [9], while the second term represents craze initiation and annihilation. Here, $A$ and $B$ are nondimensional constants. The rate $\dot{\varepsilon}_m^p$ of volumetric plastic strain is related to the hydrostatic pressure $\sigma_m$ by Kobayashi et al. [6], utilizing the preliminary finite element analysis:

$$\dot{\varepsilon}_m^p = \{(q_1 D)\cosh(q_2\sigma_m/\sigma_r)\}^{\bullet}, \tag{12}$$

where $q_1$ and $q_2$ are material constants. The craze initiation condition is also considered by the stress criterion proposed by Kawagoe and Kitagawa [4].

$$\begin{aligned} \sigma_b &\geq A_1 + (B_1/3\sigma_m), \\ \sigma_b &= \sigma_1 - v\sigma_2 - v\sigma_3, \end{aligned} \tag{13}$$

Here, $\sigma_1$, $\sigma_2$, and $\sigma_3$ are three principal stresses; $v$ is Poisson's ratio; and $A_1$ and $B_1$ are material constants. We assume $\dot{D} = 0$, if this stress criterion is not satisfied. The material parameters for this model are listed in Table 2 [6].

A matrix crack for both materials is judged at the integration point of each finite element. When $D$ approaches one, the contribution to the stiffness matrix approaches zero, and sometimes numerical instability occurs. Therefore, we eliminated the corresponding element when the averaged $D$ in the element reached $D_{cr}$. In this study, we set $D_{cr} = 0.9$. The successive elimination process yielded free nodes. For stability purposes, we searched for such nodes and excluded them from the equilibrium equations of the finite element analysis. With this procedure, we can simulate the initiation and propagation of the matrix crack.

### *2.3. Modeling of fiber breaks*

Our simulation considers fiber breaks based on the Weibull model. Potential points for the fiber break are positioned at regular intervals in the finite element model. The paths for fiber breaks are set perpendicular to the fiber axis. We set a sufficiently large number of those paths for all fiber lengths, and the interval is sufficiently small (50 μm) even for the longest fibers ($l_f$ = 2.0 mm).

Table 2. Material properties of PP matrix [6].

| | |
|---|---|
| Matrix Young's modulus $E_m$ | 1.8 GPa |
| Matrix Poisson's ratio $v_f$ | 0.33 |
| Initial yield stress $\sigma_r$ | 11.0 MPa |
| Reference strain at rehardening $\varepsilon_r$ | 0.175 |
| Reference strain rate $\dot{\varepsilon}_r$ | 0.893 (/s) |
| Rate-sensitivity parameter $m$ | 0.041 |
| Material constants | |
| Hardening rule $k_1$ | 100 |
| $k_2$ | 1.85 |
| $k_3$ | 2.37 |
| Noncoaxial angle $p_1$ | $\sin(\pi/8)$ |
| $p_2$ | 0.0001 |
| $p_3$ | 10 |
| Damage evolution law $A$ | 1.0 |
| $B$ | 0.0095 |
| Volumetric plastic strain rate $q_1$ | 0.018 |
| $q_2$ | 1.5 |

With the Weibull statistical distribution of breaking strengths, a fiber break is assumed to follow a maximum stress criterion. In the Weibull model, the cumulative failure probability of a fiber segment of length $\Delta$ is given as

$$P_f(\sigma) = 1 - \exp\left\{\left(-\frac{\Delta}{L_0}\right)\left(\frac{\sigma}{\sigma_0}\right)^{\rho}\right\}, \tag{14}$$

where $\rho$ is the Weibull modulus and $\sigma_0$ is the characteristic strength of the fiber with length $L_0$. The strength properties for glass fibers used in this study are listed in Table 3 [14]. The actual strength $\sigma_i$ for the $i$th fiber point is then chosen by selecting a random number $R_i$ within (0,1) and solving $R_i = P_f(\sigma_i, \sigma_0)$. We assign the fiber strength at each potential break point. During the simulation, fiber axial stress at the potential break points is searched. When fiber axial stress reaches the critical stress given by the Weibull model, a fiber break is introduced by eliminating the nodal force that acted on the corresponding surface.

### 2.4. *Finite element formulation*

Finally, the formulations of the finite element procedure are presented for the thermosetting and the thermoplastic composites. The virtual work for the analytical region with fiber region $V_f$ and matrix region $V_m$ is

$$\int_{V_f} \boldsymbol{\sigma} : \delta\boldsymbol{\varepsilon} dV + \int_{V_m} \boldsymbol{\sigma} : \delta\boldsymbol{\varepsilon} dV = \int_{S_t} \mathbf{f} \cdot \delta\mathbf{u} dS. \tag{15}$$

Table 3. Material properties of glass fiber [12].

| | |
|---|---|
| Young's modulus $E_f$ | 76 GPa |
| Poisson's ratio $v_f$ | 0.2 |
| Fiber radius $r_f$ | 6.5 μm |
| Weibull scale factor $\sigma_0$ | 1550 MPa |
| Gage length of the single fiber specimen $L_0$ | 24 mm |
| Weibull modulus $\rho$ | 6.34 |

Here, $\mathbf{u}$ is the displacement vector, $\mathbf{f}$ is the external force vector on the prescribed boundary $S_t$, and $\delta$ is the virtual component. We considered a quasi-static rate formulation by expanding the virtual work equation at time $t' = t + \Delta t$ around the (assumed known) state prevailing at time $t$ to linear order in $\Delta t$ as

$$\Delta t\left(\int_{V_f} {}^t\dot{\boldsymbol{\sigma}} : \delta\boldsymbol{\varepsilon} dV + \int_{V_m} {}^t\dot{\boldsymbol{\sigma}} : \delta\boldsymbol{\varepsilon} dV\right) = \int_{S_t} {}^{t'}\mathbf{f} \cdot \delta\mathbf{u} dS - \left(\int_{V_f} {}^t\boldsymbol{\sigma} : \delta\boldsymbol{\varepsilon} dV + \int_{V_m} {}^t\boldsymbol{\sigma} : \delta\boldsymbol{\varepsilon} dV\right). \quad (16)$$

In Equation (16), the constitutive law of fiber elements is given by

$$\dot{\boldsymbol{\sigma}} = \mathbf{C}_f^e : \dot{\boldsymbol{\varepsilon}} \qquad \text{for fiber}, \quad (17)$$

where $\mathbf{C}_f^e$ is the elastic constitution law of the fiber. For matrix elements, the constitutive law described above is used. This formulation was coupled with periodic-cell simulation [12] to perform simulations using the periodic-cell model. Following the routine operation employed in homogenization [13,14], for thermosetting resin, Equation (16) is then transformed into the following equation.

$$\begin{aligned} &\int_{V_f}\left(\mathbf{C}_f^e : \Delta\boldsymbol{\varepsilon}_L\right) : \delta\boldsymbol{\varepsilon} dV + \int_{V_m}\left((1-D)\mathbf{C}_m^{ep} : \Delta\boldsymbol{\varepsilon}_L\right) : \delta\boldsymbol{\varepsilon} dV \\ &= -\int_{V_f+V_m} {}^t\boldsymbol{\sigma} : \delta\boldsymbol{\varepsilon} dV + \int_{V_m} \frac{\Delta D}{1-D}({}^t\boldsymbol{\sigma} : \delta\boldsymbol{\varepsilon}) dV - \int_{V_f}\left(\mathbf{C}_f^e : \Delta\boldsymbol{\varepsilon}_G\right) : \delta\boldsymbol{\varepsilon} dV \\ &\quad - \int_{V_m}\left((1-D)\mathbf{C}_m^{ep}.\Delta\boldsymbol{\varepsilon}_G\right) : \delta\boldsymbol{\varepsilon} dV. \end{aligned} \quad (18)$$

For thermoplastic resin, Equation (16) is transformed into the following equation.

$$\begin{aligned} &\int_{V_f}\left(\mathbf{C}_f^e : \Delta\boldsymbol{\varepsilon}_L\right) : \delta\boldsymbol{\varepsilon} dV + \int_{V_m}\left((1-D)\mathbf{C}_m^{v} : \Delta\boldsymbol{\varepsilon}_L\right) : \delta\boldsymbol{\varepsilon} dV \\ &= -\int_{V_f+V_m} {}^t\boldsymbol{\sigma} : \delta\boldsymbol{\varepsilon} dV + \int_{V_m} (1-D)\frac{3\mu\Delta\bar{\varepsilon}^p \cos\delta}{\bar{\sigma}}({}^t\boldsymbol{\sigma}' : \delta\boldsymbol{\varepsilon}) dV + \int_{V_m} \frac{\Delta D}{1-D}({}^t\boldsymbol{\sigma} : \delta\boldsymbol{\varepsilon}) dV \\ &\quad - \int_{V_f}\left(\mathbf{C}_f^e : \Delta\boldsymbol{\varepsilon}_G\right) : \delta\boldsymbol{\varepsilon} dV - \int_{V_m}\left((1-D)\mathbf{C}_m^{v} : \Delta\boldsymbol{\varepsilon}_G\right) : \delta\boldsymbol{\varepsilon} dV. \end{aligned} \quad (19)$$

Here, the traction boundary $S_t$ in Equations (18) and (19) does not exist in the present periodic-cell simulation. The global strain increment $\Delta\varepsilon_G$ should be controlled to achieve various loading conditions in the periodic cell.

Finally, the discretized form of Equations (18) and (19) gives the following matrix equations. If the matrix is thermoset, the equation is

$$({}^t\mathbf{K}_f + {}^t\mathbf{K}_m)\Delta\mathbf{U}_L = -({}^t\mathbf{Q}_f + {}^t\mathbf{Q}_m) + {}^t\mathbf{Q}_{dam} - (\Delta\mathbf{Q}_{f,G} + \Delta\mathbf{Q}_{m,G}), \quad (20)$$

where

$$\mathbf{K}_f = \sum_e \int_{V_f^e} \mathbf{B}^{eT}\mathbf{D}_f^e\mathbf{B}^e dV, \quad \mathbf{K}_m = \sum_e \int_{V_m^e} (1-D)\mathbf{B}^{eT}\mathbf{D}_m^{ep}\mathbf{B}^e dV,$$

$$\mathbf{Q}_f = \sum_e \int_{V_f^e} \mathbf{B}^{eT} \hat{\boldsymbol{\sigma}} dV, \quad \mathbf{Q}_m = \sum_e \int_{V_m^e} \mathbf{B}^{eT} \hat{\boldsymbol{\sigma}} dV,$$

$$\mathbf{Q}_{\text{dam}} = \sum_e \int_{V_m^e} \frac{\Delta D}{1-D} \mathbf{B}^{eT} \hat{\boldsymbol{\sigma}} dV,$$

$$\Delta \mathbf{Q}_{f,G} = \sum_e \int_{V_f^e} \mathbf{B}^{eT} \mathbf{D}_f^e \Delta \boldsymbol{\varepsilon}_G dV, \quad \Delta \mathbf{Q}_{m,G} = \sum_e \int_{V_m^e} (1-D) \mathbf{B}^{eT} \mathbf{D}_m^{ep} \Delta \boldsymbol{\varepsilon}_G dV.$$

If the matrix is thermoplastic, the equation is

$$({}^t\mathbf{K}_f + {}^t\mathbf{K}_m)\Delta \mathbf{U}_L = -({}^t\mathbf{Q}_f + {}^t\mathbf{Q}_m) + {}^t\mathbf{Q}_v + {}^t\mathbf{Q}_{\text{dam}} - (\Delta \mathbf{Q}_{f,G} + \Delta \mathbf{Q}_{m,G}), \tag{21}$$

where

$$\mathbf{K}_f = \sum_e \int_{V_f^e} \mathbf{B}^{eT} \mathbf{D}_f^e \mathbf{B}^e dV, \mathbf{K}_m = \sum_e \int_{V_m^e} (1-D) \mathbf{B}^{eT} \mathbf{D}_m^v \mathbf{B}^e dV,$$

$$\mathbf{Q}_f = \sum_e \int_{V_f^e} \mathbf{B}^{eT} \hat{\boldsymbol{\sigma}} dV, \mathbf{Q}_m = \sum_e \int_{V_m^e} \mathbf{B}^{eT} \hat{\boldsymbol{\sigma}} dV,$$

$$\mathbf{Q}_v = \sum_e \int_{V_m^e} (1-D) \frac{3\mu \Delta \bar{\varepsilon}^p \cos\delta}{\bar{\sigma}} \mathbf{B}^{eT} \hat{\boldsymbol{\sigma}}' dV,$$

$$\mathbf{Q}_{\text{dam}} = \sum_e \int_{V_m^e} \frac{\Delta D}{1-D} \mathbf{B}^{eT} \hat{\boldsymbol{\sigma}} dV,$$

$$\Delta \mathbf{Q}_{f,G} = \sum_e \int_{V_f^e} \mathbf{B}^{eT} \mathbf{D}_f^e \Delta \boldsymbol{\varepsilon}_G dV, \text{ and}$$

$$\Delta \mathbf{Q}_{m,G} = \sum_e \int_{V_m^e} (1-D) \mathbf{B}^{eT} \mathbf{D}_m^v \Delta \boldsymbol{\varepsilon}_G dV.$$

Here, $\mathbf{U}$ is the nodal displacement vector, $\mathbf{K}_f$ and $\mathbf{K}_m$ are the tangential stiffness matrices of fiber and matrix elements, $\mathbf{Q}_f$ and $\mathbf{Q}_m$ are the nodal forces corresponding to the element

stresses, **B** is the strain-displacement matrix, **D** is the constitutive matrix, and **F** is the externally applied nodal force. The effect of the constitutive law for the matrix (Equation (7)) is included in the expression in the matrix stiffness $\mathbf{K}_m$ and the added nodal forces $\mathbf{Q}_v$ and $\mathbf{Q}_{dam}$. Here, $\Delta\mathbf{Q}_{f,G}$ and $\Delta\mathbf{Q}_{m,G}$ are the contributions by the predetermined global strain increment $\Delta\varepsilon_G$. Equations (20) and (21) are the basic equations for the present periodic-cell simulation.

With these procedures, we performed periodic-cell simulations for progressive damage. In an incremental step in the simulation, we first calculated the displacement increment $\Delta\mathbf{U}_L$ by solving Equations (20) and (21) under periodic boundary conditions. The total strain increment $\Delta\boldsymbol{\varepsilon}$ was calculated by adding the predetermined $\Delta\varepsilon_G$ to $\Delta\varepsilon_L$. Composite stress was defined as the average stress over the unit cell. In order to increase the stable time step, the rate tangent formulation of Pierce et al. [15] was used for the thermoplastic composites. In the simulations of this study, the rate of applied tensile strain was set to $1.0 \times 10^{-4}$ (/s) and time step $\Delta t$ was set to 0.1 s.

In this study, the increment of applied global strain $\Delta\varepsilon_G$ is given by

$$\Delta\boldsymbol{\varepsilon}_G = (\Delta\varepsilon_{xx}, \Delta\varepsilon_{yy}, \Delta\varepsilon_{xy})_G = \alpha(-0.3,\ 1.0,\ 0.0), \tag{22}$$

to reproduce the tensile loading condition.

## 3. Results and discussion

### 3.1. Damage growth and strength of glass fiber-reinforced thermosetting composites

Thermosetting resin is generally employed for continuous glass fiber-reinforced composites. Here, we investigated changes in strength and damage growth of glass fiber-reinforced thermosetting matrix composites with increased fiber length. Epoxy resin was assumed as a typical thermosetting resin. Material properties for fiber are listed in Table 3, and those for the matrix are listed in Table 1. The volume fraction is set as 54.2% in order to compare simulated results with experimental results for continuous glass fiber-reinforced composites. The fiber length is varied from 50 μm to 2 mm. Figure 2 presents the simulated results when the fiber length is 1 mm. A matrix crack is generated when the applied strain is 1.12%. This crack is trapped by neighboring fibers (Figure 2(b)). The fiber is then broken due to stress concentration by the matrix crack. Catastrophic failure of the composites occurs when the applied strain is 3.35%. The process of damage growth is similar to that of the continuous fiber-reinforced plastics. Figure 3 presents the simulated results when the fiber length is 200 μm. A matrix crack occurs at the fiber edges when the applied strain is 2.1%. This crack is not trapped by neighboring fibers, but it propagates into the matrix. The connections of those cracks cause catastrophic failure of the composites. Thus, when the fiber is short, the failure mode changes from fiber breaking to matrix cracking. The simulated stress–strain curves are presented in Figure 4. As the fiber becomes shorter, the maximum stress in the curve decreases. In contrast, failure strain increases due to the transition of the failure mode. The transition length of the failure mode is 200 μm. Figure 5 depicts the relationship between tensile strength and fiber length. The solid black plots denote the fiber breaking mode and open plots denote matrix cracking. When the fiber is longer than 300 μm, the strength is close to that of continuous fiber-reinforced composites. In contrast, when the fiber is shorter than 300 μm, strength decreases as fiber length decreases.

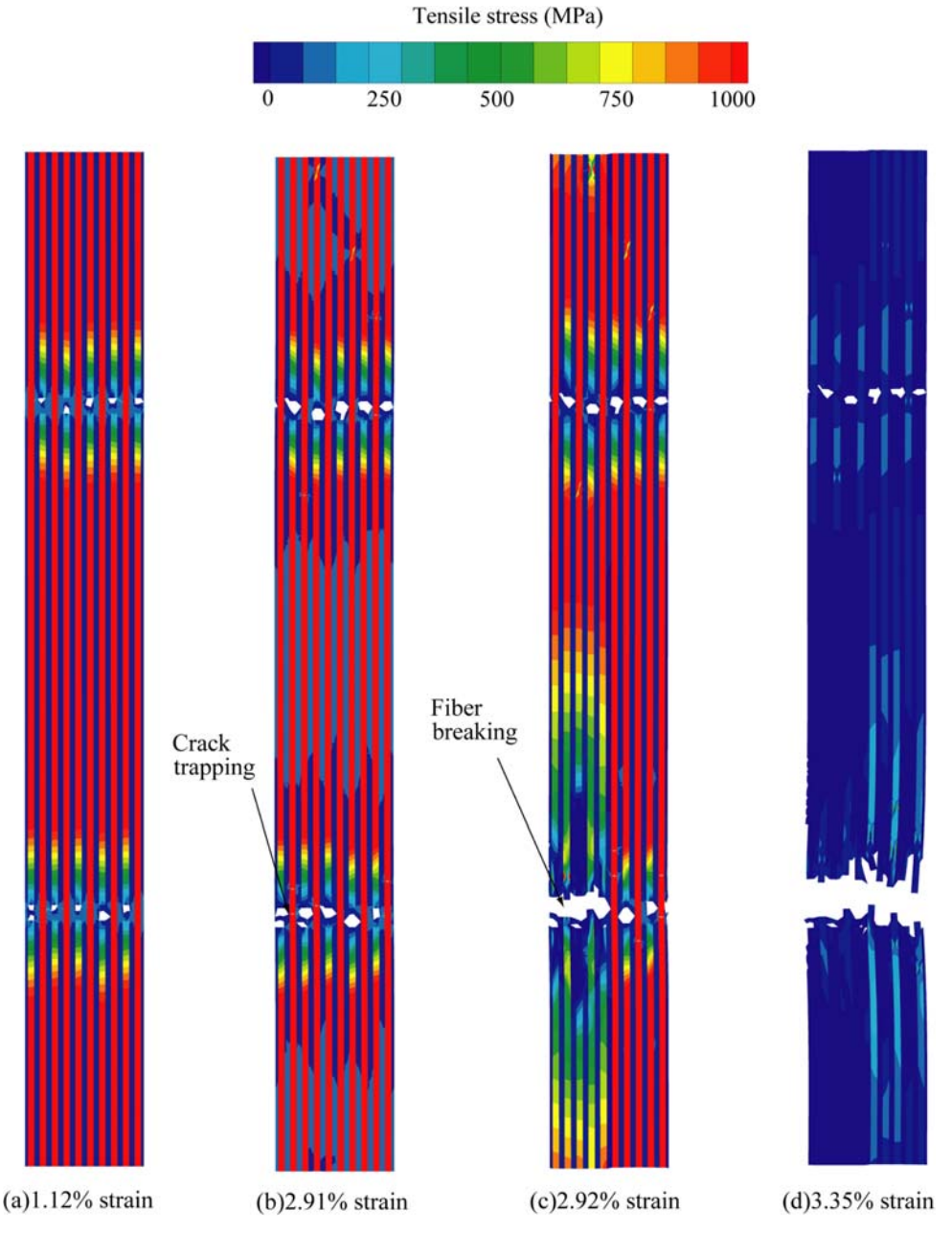


Figure 2. Simulated fracture process of glass fiber-reinforced epoxy ($L_f$ = 1 mm).

### 3.2. *Damage growth and strength of glass fiber-reinforced thermoplastic composites*

This section describes strength and damage growth of glass fiber-reinforced thermoplastic composites. Hereafter, the matrix is assumed to be PP. The material properties of PP are listed in Table 2. To compare the results for glass fiber-reinforced thermoplastic composites with those for glass fiber-reinforced thermosetting composites, the volume fraction is set as 54.2%. The simulation is performed with fiber length variation from 50 μm to 2 mm.

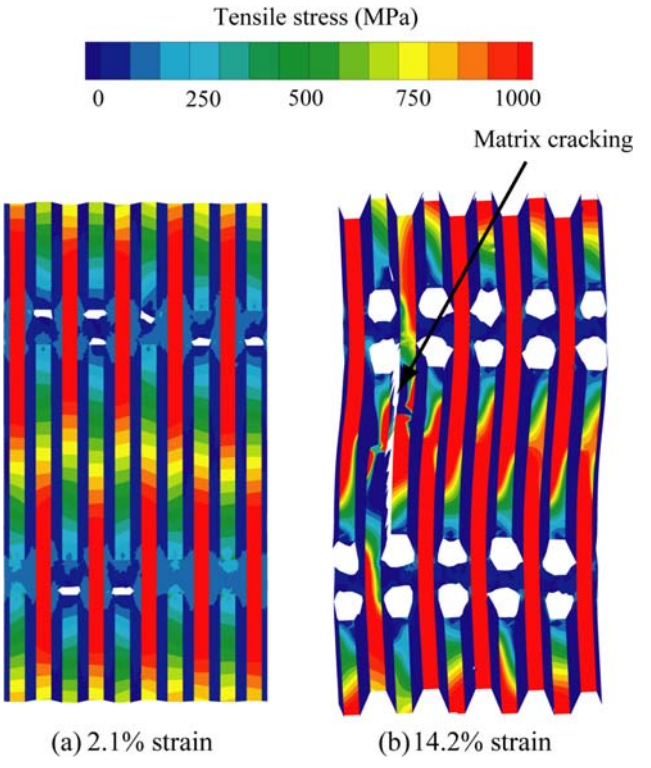


Figure 3. Simulated fracture process of glass fiber-reinforced epoxy ($L_f = 200\,\mu m$).

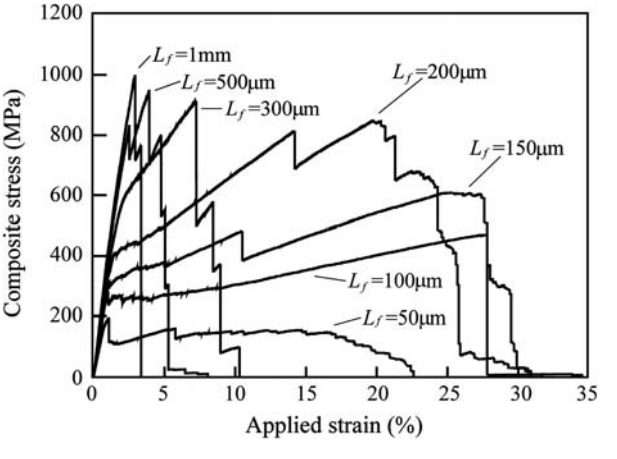


Figure 4. Stress–strain curve for glass fiber-reinforced epoxy.

Figure 6 depicts the simulated damage growth when the fiber length is 500 μm. For thermosetting resin, as described in the previous section, the main damage is fiber breaking when the fiber is longer than 300 μm. In contrast, for thermoplastic resin, the damage is matrix cracking. Figure 7 depicts the relationship between tensile strength and fiber length. As stated

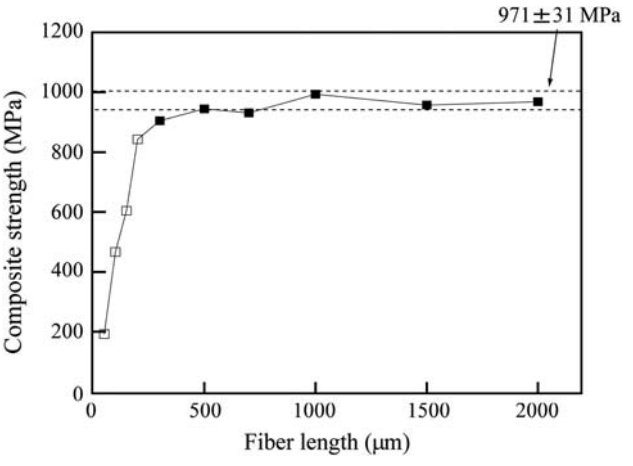


Figure 5. Composite strength vs. fiber length for glass fiber-reinforced epoxy ($V_f = 54.2\%$).

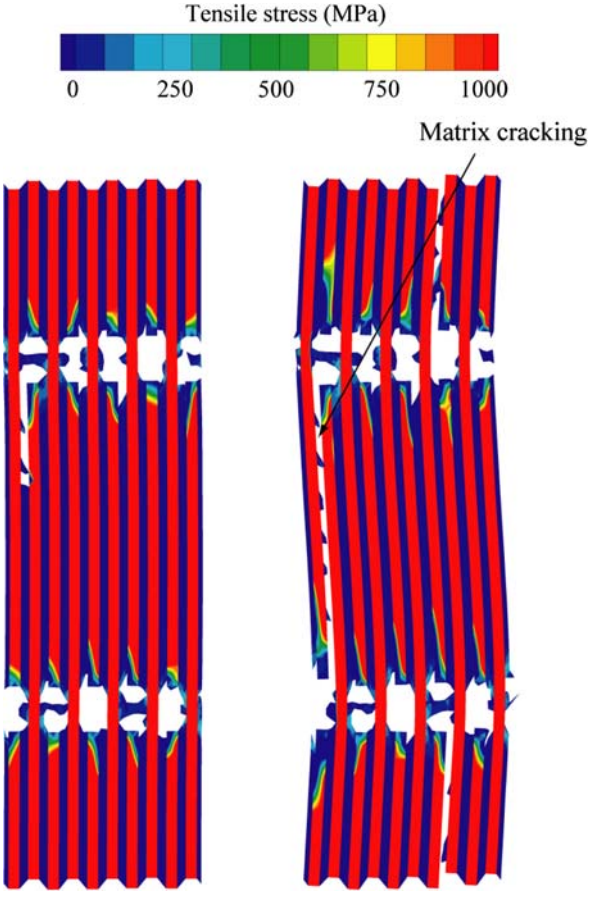


Figure 6. Simulated fracture process of glass fiber-reinforced PP ($L_f = 500\,\mu m$).

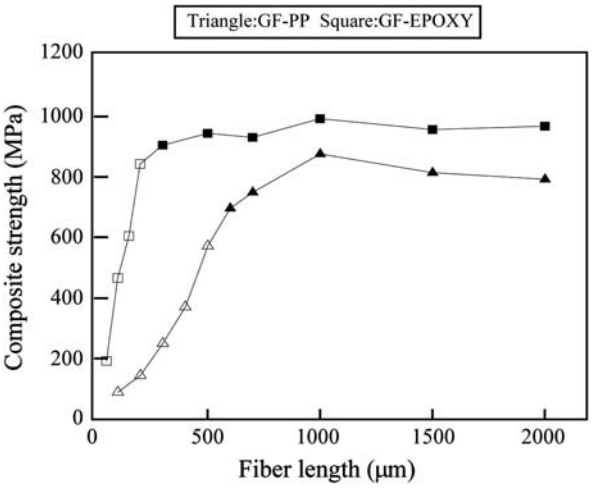


Figure 7. Composite strength vs. fiber length for glass fiber-reinforced PP ($V_f = 54.2\%$).

in the previous section, solid black plots denote fiber breaking and open plots denote matrix cracking. Strength rapidly decreases as fiber length decreases when the main damage is matrix cracking. The transition length for thermoplastic composites is 1 mm, which exceeds that for thermosetting composites. Thus, thermoplastic composites require longer fibers than thermosetting composites to improve their strength because yielding stress for thermoplastic resin (30 MPa) is much lower than that for thermosetting resin (75 MPa).

Next, the effect of volume fraction on strength and damage growth is examined. Figure 8 depicts the relationship between tensile strength and fiber length with fiber volume fractions of 5, 10, and 20%. The transition lengths are 700 μm for 20%, 1 mm for 10%, and 1.5 mm for 5%. Thus, both strength and transition length depend on the fiber volume fraction. The critical length calculated using the Kelly-Tyson model [5] is 562.8 μm. The Kelly-Tyson model yields critical length, which does not depend on the fiber volume fraction. However, the simulated transition lengths are affected by the fiber volume fraction. When the fiber volume fraction is low, the simulated transition lengths are quite different from the critical

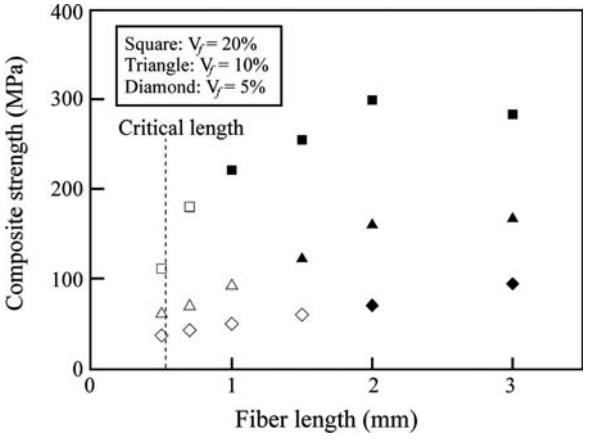


Figure 8. Composite strength vs. fiber length among various fiber volume fractions.

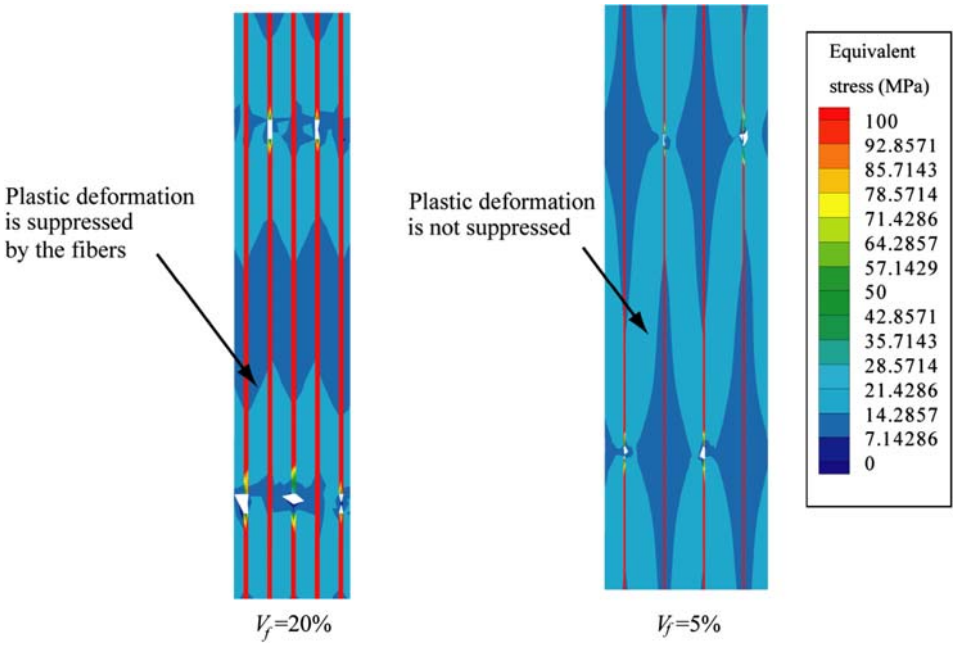


Figure 9. Equivalent stress distribution for $V_f = 20$ and 5%.

length. Figure 9 presents the simulated equivalent stress distributions for 5 and 20% fiber volume fractions. When the fiber volume fraction is 20%, the neighboring fibers prevent matrix plasticity from progressing in the composites. When the fiber volume fraction is 5%, matrix plasticity easily spreads in the composites, and thus causes an increase in simulated transition length. The simulation implies that the critical length given by Kelly-Tyson is inaccurate for estimating the transition length of the damage mode.

### 3.3. *Strength of carbon fiber-reinforced thermoplastic composites*

This section describes the simulation for carbon fiber-reinforced thermoplastic composites. We have reported on experiments for continuous carbon fiber-reinforced composites [2]. Here, we perform a simulation for this composite. The simulated composite is T700S/PP. The material properties for carbon fiber are listed in Table 4. The fiber volume fraction $V_f$ is 20% and orientation factor $\eta = 0.375$ is used. Here, the composite strength $\sigma_{\text{comp}}$ is calculated by using

$$\sigma_{\text{comp}} = \eta\{V_f\sigma_{\text{UD}} + (1 - V_f)\sigma_m\}, \tag{23}$$

Table 4. Material properties of carbon fiber.

| | |
|---|---|
| Young's modulus $E_f$ | 230 GPa |
| Poisson's ratio $v_f$ | 0.2 |
| Fiber radius $r_f$ | 3.5 μm |
| Weibull scale factor $\sigma_0$ | 4316 MPa |
| Gage length of the single fiber specimen $L_0$ | 25 mm |
| Weibull modulus $\rho$ | 5.55 |

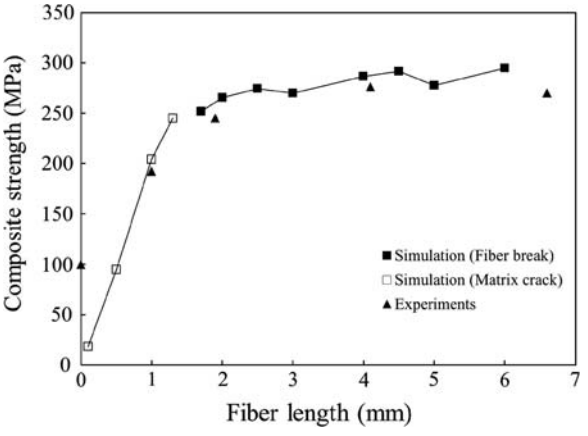


Figure 10. Composite strength vs. fiber length for carbon fiber-reinforced PP.

where $\sigma_m$ is the matrix stress and $\sigma_m = 25$ is assumed. Figure 10 illustrates the relationship between the simulated results and the experimental results. The simulated results agree well with the experimental results.

### *3.4. Rate dependence of mechanical behavior of glass fiber-reinforced thermoplastic composites*

Thermoplastic resin depends strongly on deformation rate. The energy absorption of composites also depends on deformation rate. This section investigates the rate-dependent behavior of glass fiber-reinforced thermoplastic composites.

The simulated composite is E-glass/PP. The fiber volume fraction is 10%. The strain rates used in the simulations are $1.0 \times 10^{-2}$, $1.0 \times 10^{-4}$, and $1.0 \times 10^{-6}$ (/s). Figure 11 plots the stress–strain curve when the fiber length is 100 μm. The main damage is matrix cracking. Therefore, the stress–strain curve of the composites depends strongly on the properties of the matrix and the composites depend on deformation rate. Figure 12 presents the stress–strain curve when the fiber length is 2 mm. The main damage is fiber breaking. Therefore, the

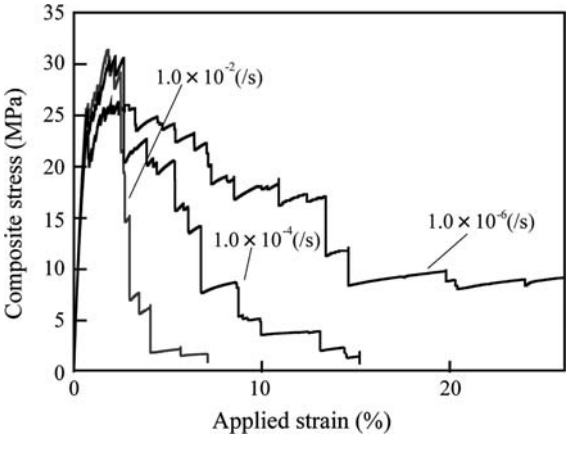


Figure 11. Effect of tensile strain rate ($L_f = 100$ μm).

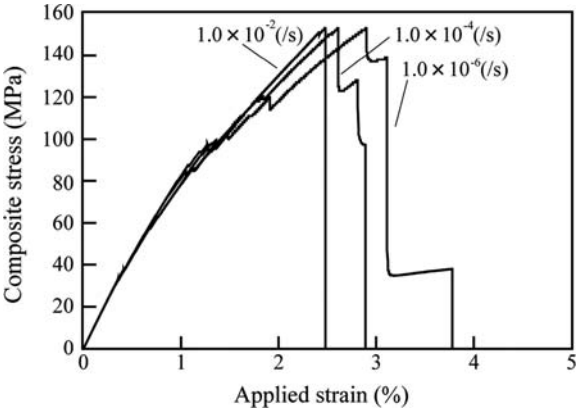


Figure 12. Effect of tensile strain rate ($L_f = 2$ mm).

stress–strain curve of the composites depends strongly on the properties of the fiber and the composites do not depend on deformation rate.

Therefore, matrix properties can be changed to improve the rate dependence only when the fiber is short.

## 4. Conclusions

This study addresses tensile damage growth in fiber-reinforced plastic composites with a periodic unit-cell simulation that considers the constitutive law of the matrix, matrix cracking, and fiber breaking. In this simulation, thermoplastic or thermosetting resin is assumed as a matrix. The effects of fiber length, matrix and fiber properties, and fiber volume fraction on damage growth and strength are investigated. The obtained conclusions are summarized as follows.

(1) Tensile damage growth and strength of discontinuous fiber-reinforced thermosetting composites are investigated. When the fiber length is 300 μm, the main damage mechanism transitions from matrix cracking to fiber breaking. The strength of discontinuous fiber-reinforced composites tends to approach that of continuous fiber-reinforced composites as the fiber length increases. If the fiber is shorter than 300 μm, strength drastically decreases as the fiber length decreases.
(2) Tensile damage growth and strength of discontinuous glass fiber-reinforced thermoplastic composites are investigated. The transition length is shorter than that of thermosetting composites because the yielding stress of thermoplastic resin is lower than that of thermosetting resin.
(3) The effect of volume fraction on the failure and damage of discontinuous glass fiber-reinforced thermoplastic composites is investigated. Results indicate that both strength and transition length depend on the fiber volume fraction. The critical length calculated using the Kelly-Tyson model is inappropriate for estimating transition length because critical length does not depend on the fiber volume fraction.
(4) We compare the simulated results with those of experiments for discontinuous carbon fiber-reinforced thermoplastic composites. The simulated results agree with experiments.
(5) The deformation rate dependence of the mechanical behavior of glass fiber-reinforced thermoplastic composites is investigated. When the fiber length is 100 μm, the stress–

strain curve of the composites strongly depends on the properties of the matrix. In contrast, when the fiber length is 2 mm, the behavior of composites is independent of deformation rate.

## Acknowledgments

We would like to acknowledge the support of the New Energy and Industrial Technology Development Organization (NEDO) (Project No. P08024). T. O. acknowledges the support of the Ministry of Education, Culture, Sports, and Science and Technology of Japan under Grants-in-Aid for Scientific Research No. 22360352.



## References

[1] Guedes JM, Kikuchi N. Preprocessing and postprocessing for materials based on the homogenization method with adaptive finite element methods. Computer Methods in Applied Mechanics and Engineering. 1990;83:143–98.
[2] Hashimoto M. Research and development on strength improvement of discontinuous carbon fiber reinforced plastics [Doctoral dissertation]. Tohoku University (in Japanese); 2012.
[3] Huang H, Talreja R. Numerical simulation of matrix micro-cracking in short fiber reinforced polymer composites: initiation and propagation. Composites Science and Technology. 2006;66:2743–57.
[4] Kawagoe M, Kitagawa M. Craze initiation in poly(methyl methacrylate) under biaxial stress. Journal of Polymer Science Polymer Physics Edition. 1981;19:1423–33.
[5] Kelly A. Strong solids. Oxford: Clarendon Press; 1966. p. 131.
[6] Kobayashi S, Tomii D, Shizawa K. A modelling and simulation on failure prediction of ductile polymer based on craze evolution and annihilation. Transactions of the Japan Society of Mechanical Engineers A. 2004;70:810–7, in Japanese.
[7] Matous K, Geubelle PH. Multiscale modeling of particle debonding in reinforced elastomers subjected to finite deformations. International Journal for Numerical Methods in Engineering. 2006;65:190–223.
[8] Murakami S, Ohno N. A continuum theory of creep and creep damage. Creep in structures. Berlin: Springer-Verlag; 1981. 422–44.
[9] Murakami D. Kobayashi S. Torigaki T. Shizawa K. A thermomechanical modeling and simulation of viscoplastic large deformation behavior for polymeric materials: 2nd report, vertex model based on flow rule and its finite element analysis. Transactions of the Japan Society of Mechanical Engineers A. 68: 682–9 (in Japanese); 2002.
[10] Nishikawa M. Multiscale modeling for the microscopic damage and fracture of fiber reinforced plastic composites [Dr Eng. Thesis]. The University of Tokyo (in Japanese); 2008.
[11] Nishikawa M, Okabe T, Takeda N. Periodic-cell simulations for the microscopic damage and strength properties of discontinuous carbon fiber reinforced plastic composites. Advanced Composite Materials. 2009;18:77–93.
[12] Okabe T, Nishikawa M, Takeda N. Micromechanics on the rate-dependent fracture of discontinuous fiber-reinforced plastics. International Journal of Damage Mechanics. 2010;19:339–60.
[13] Okabe T, Nishikawa M, Toyoshima H. A periodic unit-cell simulation of fiber arrangement dependence on the transverse tensile failure in unidirectional carbon fiber reinforced composites. International Journal of Solids and Structures. 2011;48:2948–59.
[14] Okabe T, Takeda N. Elastoplastic shear-lag analysis of single-fiber composites and strength prediction of unidirectional multi-fiber composites. Composites A. 2002;33:1327–35.
[15] Ohno N, Okumura D, Noguchi H. Microscopic symmetric bifurcation condition of cellular solids based on a homogenization theory of finite deformation. Journal of the Mechanics and Physics of Solids. 2002;50:1125–53.
[16] Pierce D, Shih CF, Needleman A. A tangent modulus method for rate dependent solids. Computers & Structures. 1984;18(5):875–87.
[17] Rice JR, Tracey DM. On the ductile enlargement of voids in triaxial stress fields. Journal of the Mechanics and Physics of Solids. 1969;17:201–17.